Plastic joining of open-cell nickel foam and polymethyl methacrylate (PMMA) sheet by friction stir incremental forming

Journal of Materials Processing Tech. 282 (2020) 116691

Contents lists available at ScienceDirect

Journal of Materials Processing Tech.

journal homepage: www.elsevier.com/locate/jmatprotec

Plastic joining of open-cell nickel foam and polymethyl methacrylate (PMMA) sheet by friction stir incremental forming

Ryo Matsumoto[a,*], Harutaka Sakaguchi[a], Masaaki Otsu[b], Hiroshi Utsunomiya[a]

[a] Division of Materials and Manufacturing Science, Osaka University, 2-1 Yamadaoka, Suita 565-0871, Japan
[b] Department of Mechanical Engineering, Faculty of Engineering, University of Fukui, 3-9-1 Bunkyo, Fukui 910-8507, Japan

ARTICLE INFO

Associate Editor: M Merklein

Keywords:
Dissimilar joining
Friction heating
Incremental forming
Nickel foam
Polymethyl methacrylate (PMMA)
Composite structural component

ABSTRACT

Friction stir incremental forming (FSIF) process was applied to join a commercial open-cell type nickel foam with a polymethyl methacrylate (PMMA) sheet for fabrication of porous metal–nonporous resin composite. In this process, a rotating rod-shaped tool was vertically pushed and horizontally fed against the sheet on the foam. The sheet was frictionally heated and incrementally deformed by the rotating tool, while the cellular matrix of the foam was not plastically deformed. The sheet with a thickness of 1.0 mm was joined with the foam under FSIF conditions of rotation rate faster than 2000 rpm and feed rate slower than 60 mm/min. The joining strength between the foam and the sheet was investigated by performing tensile test. The joining strength was obtained over the fracture strength of the foam. The joining mechanism of the foam and the sheet was discussed from the microscopic observation of the foam–sheet interface and the temperature change in the sheet. It is concluded that the sheet was mechanically interlocked (anchored) to the porous structure of the foam by the plastic flow of the heated and softened PMMA into the surface pores of the foam.

1. Introduction

To realize lightweight structural components, the use of porous materials has one of attractive and practical means owing to their low density. Ashby et al. (2000) and Banhart (2001) have introduced the characterization, properties, manufacturing methods and applications of porous materials. Their porous structures have potentials for contributing to not only lightweight but also functional features such as high energy absorbing capacity, low heat transfer property and high sound absorbing capacity. Composite components with porous material and nonporous material such as sandwich-structure composite play an important role for the more widespread use of porous materials in structural and/or functional components. In fabrication of the composite components, joining of porous material and nonporous material is a crucial technical target. Since the porous structures tend to exhibit low specific strength characteristics, joining with high specific strength material such as resin is strongly desired for improving the strength–-mass relationship in a sandwich-structured composite.

Some fabrication methods for the porous–nonporous metal composite were proposed for porous materials. Peng et al. (2019) joined a closed-cell type aluminum foam with an aluminum sheet by friction stir welding (FSW). In this method, the foam was stirred with the sheet by a tool with a probe. Liu et al. (2017) joined open-cell type nickel, copper and iron-nickel foams with aluminum alloy sheet by self-piercing riveting. Wang et al. (2010) fabricated an open-cell type aluminum foam with an aluminum alloy sheet by vibration aided liquid phase bonding. Shiomi et al. (2010) fabricated a closed-cell type aluminum foam with a stainless steel pipe by molding the foam into the pipe. Lobos et al. (2009) and Koriyama et al. (2012) closed surface pores of a lotus-type porous copper by wire-brushing and shot-peening processes. The authors (Matsumoto et al., 2015, 2018) applied friction stir incremental forming (FSIF) process for sheet metal forming to form nonporous skin layer on a surface of a closed-cell type aluminum foam. Concerning fabrication methods for porous metal–nonporous nonmetal composite, Kitazono et al. (2009) and Yuan et al. (2015) coated epoxy resin on a closed-cell type aluminum foam. The authors (Matsumoto et al., 2016) also filled surface pores of a closed-cell type aluminum foam with polyamide by selective laser melting (SLM). Suzuki et al. (2018) infiltrated epoxy resin into open-cell surface layer of aluminum, while Kim et al. (2019) joined an aluminum alloy sheet with polyamide through porous surface layer of the aluminum sheet by hot pressing. The strength–mass relationship of above sandwich-structured composites was reported to be improved in tensile, compression and bending tests.

Many joining methods for nonporous metal and resin sheet were developed. For example, Katayama and Kawahito (2008) joined a

* Correspnding author.
E-mail address: ryo@mat.eng.osaka-u.ac.jp (R. Matsumoto).

https://doi.org/10.1016/j.jmatprotec.2020.116691
Received 1 February 2020; Received in revised form 17 March 2020; Accepted 24 March 2020
Available online 31 March 2020
0924-0136/

Table 1
Some research works of fabrication processes for composites of porous metal, nonporous metal and nonporous nonmetal.

Composite	Fabrication process	Material a (substrate)	Material b	Forming/heating material(s)	Remark	Reference(s)
Porous metal–nonporous metal	Friction stir welding (FSW)	Closed-cell type aluminum foam	Aluminum sheet	Materials a and b		Peng et al. (2019)
	Self-piercing riveting (SPR)	Open-cell type nickel, copper and iron-nickel foams	Aluminum alloy sheet	Materials a and b		Liu et al. (2017)
	Vibration aided bonding	Open-cell type aluminum foam	Aluminum alloy sheet	Interlayer material (Zn-Al-Cu based filler alloy)		Wang et al. (2010)
	Extrusion and molding	Stainless steel pipe	Closed-cell type aluminum foam	Material b	No joining	Shiomi et al. (2010)
	Wire-brushing	Lotus-type porous copper	–	Material a	Closure of surface pores	Lobos et al. (2009)
	Shot-peening	Lotus-type porous copper	–	Material a	Closure of surface pores	Koriyama et al. (2012)
	Friction stir incremental forming (FSIF)	Closed-cell type aluminum foam	–	Material a	Closure of surface pores	Matsumoto et al. (2015)
	Friction stir powder incremental forming (FSPIF)	Closed-cell type aluminum foam	Aluminum powder	Materials a and b		Matsumoto et al. (2018)
Porous metal–nonporous nonmetal	Infiltration	Closed-cell type aluminum foam	Epoxy resin	Material b		Kitazono et al. (2009); Yuan et al. (2015)
	Selective laser melting (SLM)	Closed-cell type aluminum foam	Polyamide powder	Material b		Matsumoto et al. (2016)
	Infiltration	Aluminum with open-cell surface layer	Epoxy resin	Material b		Suzuki et al. (2018)
	Hot pressing	Aluminum alloy sheet with porous surface layer	Polyamide sheet	Material b		Kim et al. (2019)
Nonporous metal–nonporous nonmetal	Laser irradiation	Stainless steel plate	Polyethylene terephthalate (PET) sheet	Materials a and b		Katayama and Kawahito (2008)
	Friction lapping	Aluminum alloy sheet	Ethylene-acrylic acid copolymer (EAA) sheet	Material a		Okada et al. (2014)
	Injection molding	Aluminum alloy sheet with micro-blasted surface texture	Polybutylene terephthalate (PBT)	Material b		Kajihara et al. (2018)

stainless steel plate with a polyethylene terephthalate (PET) plastic sheet by irradiating diode laser irradiation onto the PET sheet. In this method, joining was realized by atomic, nanostructural or molecular bonding through the oxide film of stainless steel. Okada et al. (2014) developed friction lap processing of which an aluminum alloy sheet was welded with an ethylene-acrylic acid copolymer (EAA) sheets by pressing a probe less rotating tool from the surface of the aluminum sheet. Kajihara et al. (2018) developed blast-assisted direct joining of which an aluminum alloy sheet with micro-blasted surface texture was joined with polybutylene terephthalate (PBT) by injecting the PBT to the aluminum sheet on molding in the mold. In these joining processes, the metal was mechanically joined with the resin by the micro surface topology of the metal or the resin. These fabrication processes for the composites are summarized in Table 1.

In this study, friction stir incremental forming (FSIF) process is applied to join a commercial open-cell type nickel foam with a polymethyl methacrylate (PMMA) sheet for fabrication of porous metal–nonporous resin composite. The relationship between the FSIF conditions and the deformation behavior of the sheet is investigated. The joining strength between the foam and the sheet is investigated by performing tensile test. The joining mechanism of the foam and the sheet is discussed from the microscopic observation of the foam–sheet interface and the temperature change in the sheet.

2. Joining of porous material and resin by friction stir incremental forming

FSIF process which was originally developed for sheet metal forming by Otsu et al. (2010) is a forming process combining single point incremental sheet forming with friction stir welding (FSW). The authors (Matsumoto et al., 2015, 2018) applied FSIF process to form nonporous skin layer on a surface of a closed-cell type aluminum foam. In this study, FSIF process is applied to join porous material with resin sheet for fabrication of porous metal–nonporous resin composite. Fig. 1 shows the schematic illustration of FSIF process for joining of porous material and resin sheet. A rotating rod-shaped tool is vertically pushed against the sheet placed on the foam and horizontally fed into the sheet. The tip of the tool is flat. The tool is not tilted with respect to the z axis. The sheet is aimed to be frictionally heated and incrementally deformed by the rotation and feed of the tool, while the foam is not plastically deformed.

3. Experimental procedures

3.1. Nickel foam and polymethyl methacrylate

A commercial open-cell type nickel foam (Sumitomo Electric Industries: Celmet®, Ni-Cr, Fig. 2) (Inazawa et al., 2010) was used as porous material for FSIF process. The mean pore diameter, mean apparent density and mean buoyant density of the foam were 0.8 mm, $\rho_f = 0.42\,Mg/m^3$ and $5.50\,Mg/m^3$, respectively (Kim et al., 2017). However, the pores with various sizes and shapes were randomly distributed in the foam. The porosity was calculated to be greater than 0.9 from the apparent density and the buoyant density. Here it implies that the micro pores exist in cellular matrix because the buoyant density was lower than the density of pure nickel ($8.90\,Mg/m^3$). The average plateau stress of the foam was $\sigma_{pl} = 0.42$ MPa (Kim et al., 2017).

A commercial transparent polymethyl methacrylate (PMMA) sheet with a thickness of 1.0 mm (Asahi Kasei Chemicals Corporation: Delaglass™ A) was used as resin for FSIF process. The surface of the sheet used was as-received condition (surface roughness: $Ra = 0.04$ μm). The density of the sheet was $\rho_s = 1.19\,Mg/m^3$, and the glass transition temperature was 373 K. The proof stress of the sheet was $\sigma_s = 75$ MPa. The sheet was put on the foam before FSIF process.

Since the specific proof stress of the sheet ($\sigma_s/\rho_s = 63\,MPa{\cdot}m^3/Mg$) is much higher than the specific plateau stress of the foam ($\sigma_{pl}/\rho_f = 1\,MPa{\cdot}m^3/Mg$), the strength of the foam–sheet composite is expected to be higher than that of the foam. Therefore the fabrication of the foam joined with the sheet is effective for improving the specific strength of the component with foam. In addition, it has a potential for improving the functional properties such as anti-corrosion and high airtightness properties.

3.2. Friction stir incremental forming (FSIF) conditions

The nickel foam with a rectangular parallelepiped with the dimensions of 20 mm x 20 mm x 10 mm and the PMMA sheet with a length of 60 mm and a width of $w_s = 20$ mm were used for FSIF process. FSIF process was performed under dry condition (without lubrication) at room temperature on a 3-axis NC milling machine (Roland DG Corporation: MDX-540 s). The rod-shaped tool with a surface roughness of $Ra = 1.6$ μm was made of a high speed tool steel (JIS: SKH51, 58 HRC). The tool diameter was φ6 mm, and the tip was flat with a corner radius of 1 mm as illustrated in Fig. 1. Therefore the diameter of the flat area was d_e = φ4 mm. The FSIF conditions were set as follows; the rotation rate of the tool was $\omega = 1000$–12,000 rpm, the pushing pitch (pushing depth) in the z direction was $p_z = 0.5$ mm, the feed rate of the tool was $f = 6$–600 mm/min in the y direction. Here the pushing pitch

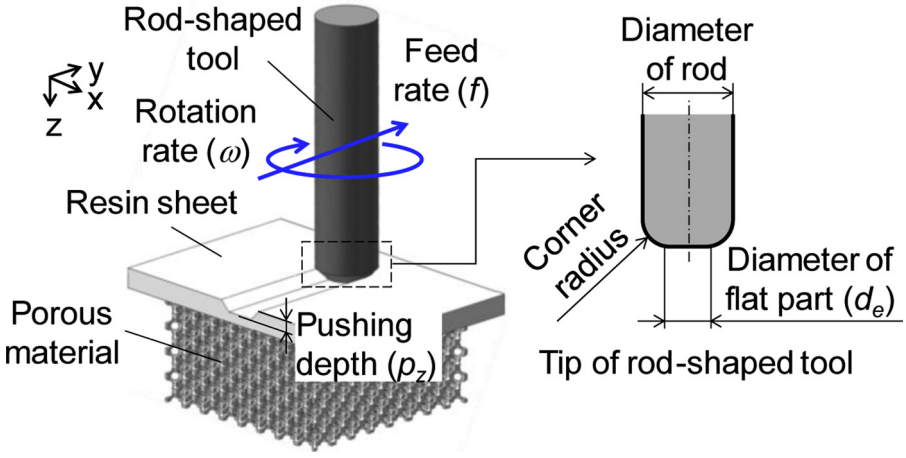

Fig. 1. Schematic illustration of friction stir incremental forming (FSIF) process for joining of porous material and resin sheet.

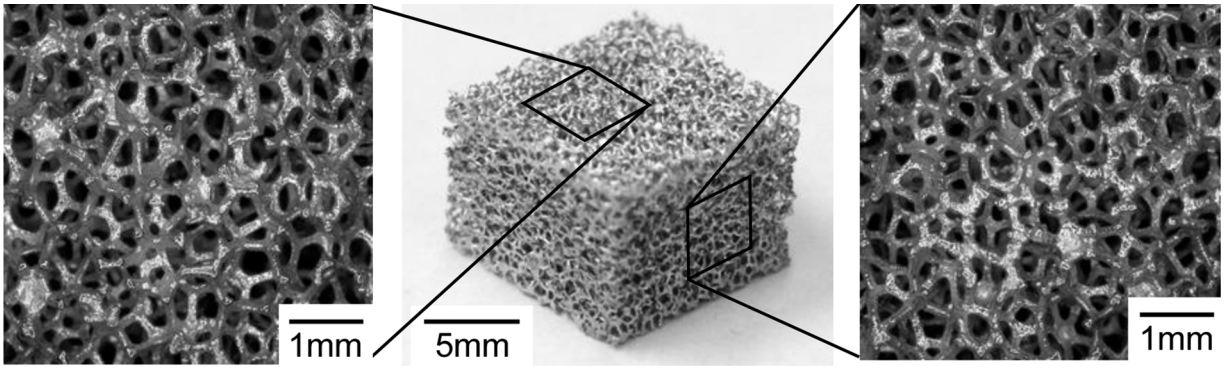

Fig. 2. Photographs of open-cell nickel foam used in this study.

(pushing depth) was a pitch (depth) in the z direction from the top surface of the formed PMMA sheet.

3.3. Tensile test conditions

The joining strength of the nickel foam–PMMA sheet joined by FSIF process was measured by performing uniaxial tensile test on a material testing machine. The top surface of the joined area of the sheet was bonded with a PMMA rod with a diameter of φ6 mm and a length of 50 mm by a dichloromethane solvent after polishing and degreasing of the top surface of the joined area of the sheet. On the other hand, the bottom of the foam was bonded with a steel plate by an epoxy adhesive, and the foam was fixed from the top of the foam to the plate using jigs with bolts. The schematic illustration of the foam–sheet specimen bonded with rod and plate for uniaxial tensile test is shown in Fig. 3. The bonding strengths of the sheet–rod and the foam–plate were approximately 10 MPa and 30 MPa, respectively. The rod–-sheet–foam–plate specimen was pulled perpendicular to the joined interface of the foam–sheet with a rate of 1 mm/min at room temperature by chucking the rod and the plate on a material testing machine.

The joining strength of the foam and the sheet was evaluated by nominal tensile stress. The nominal tensile stress (σ_t) was calculated by dividing the tensile load by the nominal surface area of the sheet in FSIF process ($d_e \cdot w_s$).

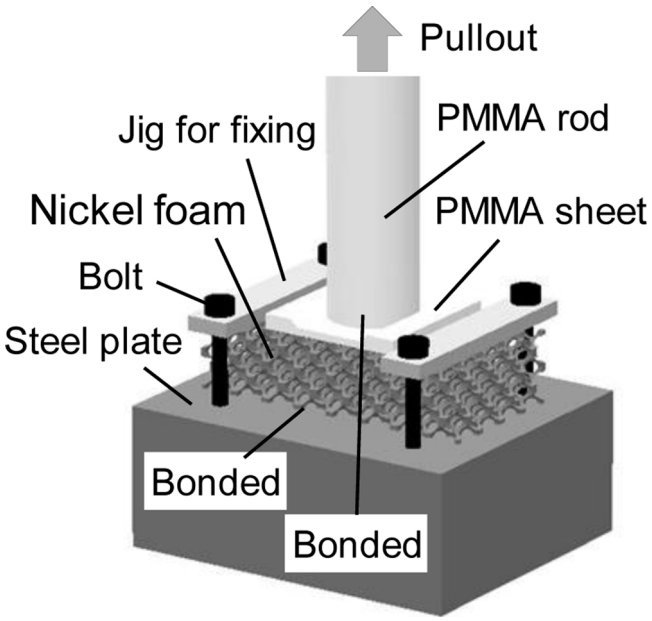

Fig. 3. Schematic illustration of specimen of nickel foam–PMMA sheet bonded with PMMA rod and steel plate for uniaxial tensile test.

4. Experimental results

4.1. Relationship between FSIF conditions and joining state

Fig. 4 shows the appearances of the specimen of the nickel foam and the PMMA sheet after FSIF process. The surface of the FSIFed area in the PMMA sheet (width in the x direction: approximately 5 mm) was clouded, and rotation marks and scanning marks of the rod-shaped tool appeared. The sheet was joined with the foam in Fig. 4(a), and the width of the clouded area in the x direction was almost constant. On the other hand, the sheet was not joined with the foam in Fig. 4(b)–(d). Due to high tool feed rate, the plastic deformation of the sheet was unstable, so that the width of the clouded area was not constant in the x direction in Fig. 4(b). Due to low tool rotation rate, the turbidity of the FSIFed area in the sheet was low in Figs. 4(c) and (d). The surface profiles of the PMMA sheet after FSIF process are shown in Fig. 5. The sheet of the FSIFed areas of (a) and (c) were concaved under low feed rate condition ((a) and (c)) because the sheet was pushed into the foam.

Fig. 6 shows the x–z cross-sectional photographs of the interface between the nickel foam and the PMMA sheet after FSIF process. In Fig. 6(a), in which the sheet was joined with the foam, PMMA plastically flowed into the porous structure of the foam below the FSIFed area of the sheet, and the foam below the FSIFed area was not plastically deformed. The foam below the FSIFed area was not also plastically deformed in Fig. 6(b), however the top surface of the sheet was shaved, and the gap was observed between the foam and the sheet at the FSIFed area. As the result, the sheet was not joined with the foam. On the other hand, in Fig. 6(c) and (d), in which the sheet was not also joined with the foam, the sheet and the foam were plastically deformed and the bottom part of the sheet did not plastically flow into the porous structure of the foam.

The experimental results of the joining state of the foam–sheet specimen after FSIF process are plotted against the relationship between the rotation rate and the feed rate of FSIF process in Fig. 7. The sheet was joined with the foam under FSIF conditions of $\omega \geq 2000$ rpm and $f \leq 60$ mm/min. The sheet was not joined with the foam under FSIF conditions of $\omega \leq 1000$ rpm due to the deformation of the foam and $f \geq 120$ mm/min due to the gap between the foam and the sheet.

The measurement results of the flow thickness of PMMA into the porous structure of the foam are shown in Fig. 8. Here the flow thickness was measured in the x–z cross-section of the center of the y direction in the fabricated foam joined with sheet at 1.0 mm pitch in the x direction by microscopic observation. The variations in tool rotation and feed rates of FSIF conditions were summarized by the relative forming rate ($r\omega/f$). The relative forming rate is known to be an index of heat input in friction stir welding process (Lakshminarayanan et al., 2009). The flow thickness of PMMA in the foam joined with the PMMA sheet was thicker than 0.2 mm, especially it was 0.6–0.7 mm in the FSIF conditions of $r\omega/f \geq 1500$. The flow thickness of PMMA in the foam was classified by two types; thicker than 0.2 mm (joining) and thinner than

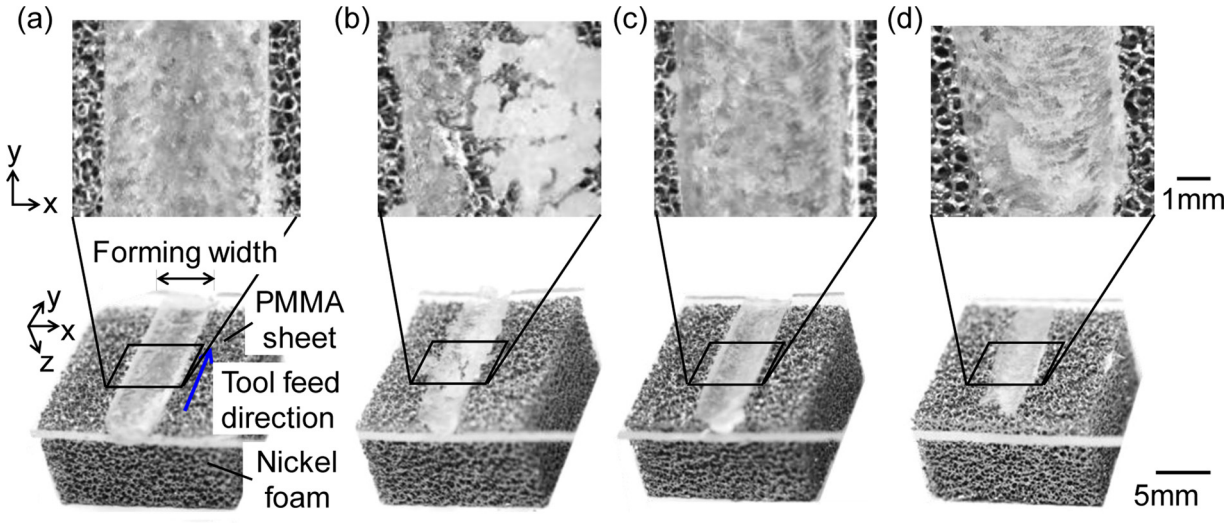

Fig. 4. Appearances of nickel foam and PMMA sheet after FSIF process: (a) ω = 6000 rpm, f = 10 mm/min (joining), (b) ω = 6000 rpm, f = 120 mm/min (no joining), (c) ω = 1000 rpm, f = 10 mm/min (no joining), (d) ω = 1000 rpm, f = 120 mm/min (no joining).

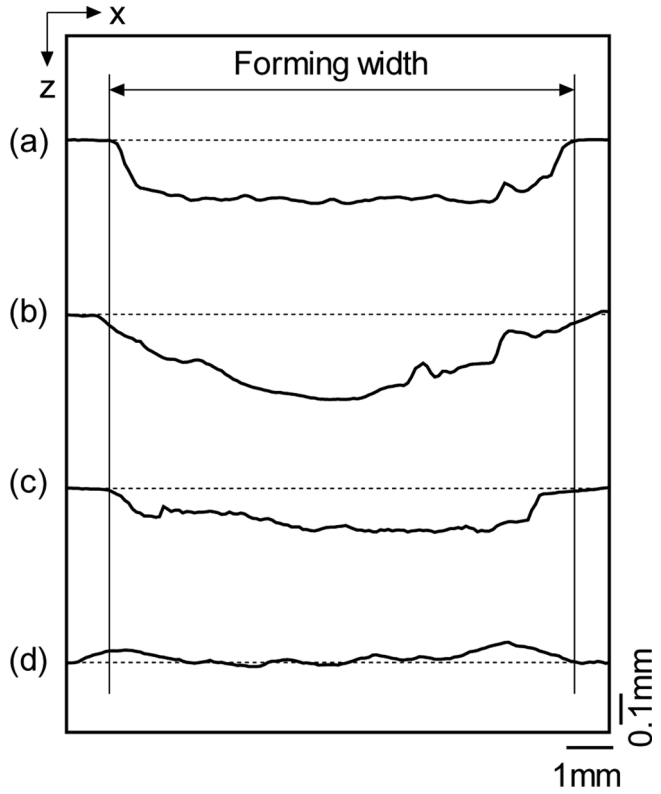

Fig. 5. Surface profiles of PMMA sheet after FSIF process: (a) ω = 6000 rpm, f = 10 mm/min (joining), (b) ω = 6000 rpm, f = 120 mm/min (no joining), (c) ω = 1000 rpm, f = 10 mm/min (no joining), (d) ω = 1000 rpm, f = 120 mm/min (no joining).

0.05 mm (no joining) in the FSIF conditions of $r\omega/f \leq 500$. The joining state of the foam–sheet specimen after FSIF process was unstable because the FSIF conditions of $r\omega/f \leq 500$ corresponded to low rotation rate condition or high feed rate condition.

4.2. Joining strength of nickel foam and PMMA sheet

Fig. 9 shows the photographs of the interface of the nickel foam and the PMMA sheet during tensile test. The sheet whose bottom part flowed into the porous structure of the foam was pulled from the porous structure of the foam in the interface with a flow thickness of PMMA of 0.5 mm. In this case, the cellular matrix of the foam was not fractured, and the sheet was detached from the foam. On the other hand, the cellular matrix of the foam was fractured in the interface with a flow thickness of PMMA of 0.7 mm, however the sheet was partly kept to be joined with the foam. The nominal tensile stress–pullout stroke curves of the foam and the sheet in tensile test were shown in Fig. 10. Here each test was carried out with two specimens joined under the same condition. The joining strength (nominal tensile stress) of the foam joined with the sheet increased with increasing flow thickness of PMMA, and the joining strength was much higher than the plateau stress of the foam. Especially the joining strength with a flow thickness of PMMA of 0.7 mm was $\sigma_t > 7.0$ MPa over the fracture strength of the foam because the cellular matrix of the foam was fractured with joining of the foam and the sheet.

From above results, mechanical interlock of the PMMA sheet flowed into the porous structure of the foam was dominant in the joining strength of the foam and the sheet.

4.3. Minimum pushing depth of tool and maximum thickness of PMMA sheet for joining

Influence of the pushing depth of the rod-shaped tool and the PMMA sheet thickness on the joining state was investigated under FSIF conditions with ω = 6000 rpm and f = 10 mm/min. Fig. 11 shows the relationship between the pushing depth and the joining state in FSIF process with a sheet thickness of 1.0 mm. The sheet was joined under $p_z \geq 0.5$ mm (also shown in Fig. 6), however the cellular matrix of the foam was slightly deformed under $p_z = 0.7$ mm. On the other hand, the sheet was not joined under $p_z \leq 0.3$ mm.

Fig. 12 shows the relationship between the sheet thickness and the joining state in FSIF process with $p_z = 0.5$ mm. The sheet thinner than 1.5 mm was joined without deforming the cellular matrix of the foam, while the sheet thicker than 2.0 mm was not joined. Multi pass operation in the z direction and rod-shaped tool with a larger diameter may be effective for joining of a thick sheet.

4.4. Crystallinity and hardness of PMMA sheet after FSIF process

Fig. 13 shows the x-ray diffraction (XRD) pattern of the formed surface of the PMMA sheet after FSIF process. The XRD pattern was measured by x-ray diffraction method on an x-ray diffractometer (Rigaku Corporation: SmartLab SE) under an irradiation power of 1.6 kW

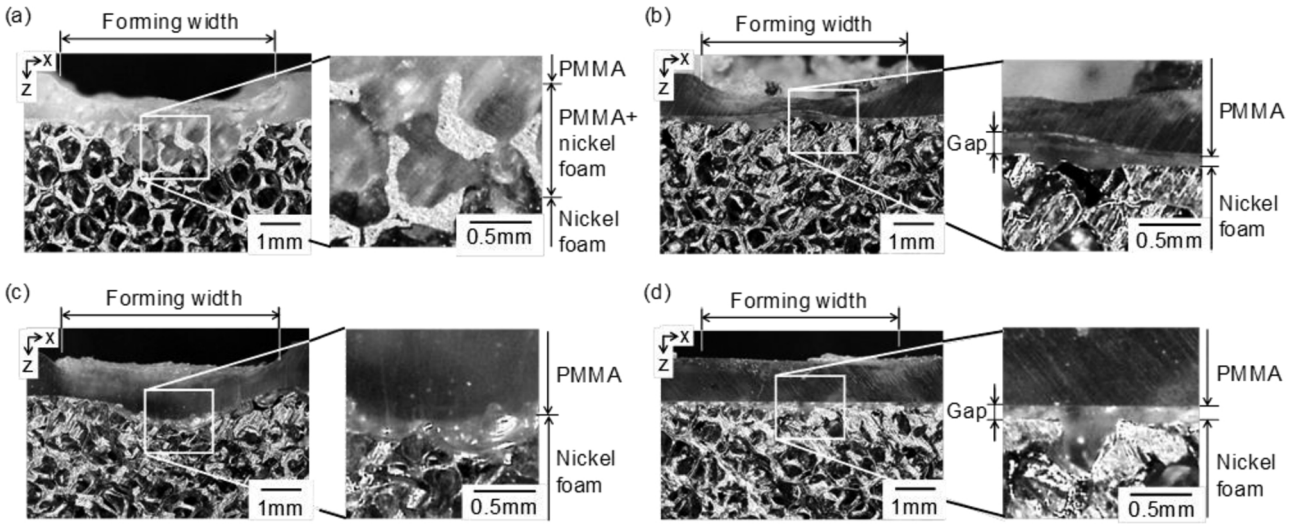

Fig. 6. Photographs of x–z cross-section of interface of nickel foam–PMMA sheet after FSIF process: (a) ω = 6000 rpm, f = 10 mm/min (joining), (b) ω = 6000 rpm, f = 120 mm/min (no joining), (c) ω = 1000 rpm, f = 10 mm/min (no joining), (d) ω = 1000 rpm, f = 120 mm/min (no joining).

and diffraction angles of 5–70°. The diffraction angles of the peak intensity of the FSIFed sheets were the same with the as-received sheet. The sharp peaks of the intensity were not measured in the diffraction pattern of all sheets because PMMA was amorphous resin. The peak intensities of the diffraction pattern of the FSIFed sheets were lower than that of the as-received sheet. The crystallinity of the sheet was reduced by FSIF process, however the influence of the FSIF conditions (tool rotation and feed rates) on the reduction of the crystallinity was small. The Rockwell's hardness of the formed surface of the PMMA sheet after FSIF process is shown in Fig. 14. The hardness of the FSIFed sheets was almost the same with the as-received sheet.

5. Discussions on joining mechanism

5.1. Temperature increase of PMMA sheet

The temperature change of the PMMA sheet during FSIF process was measured by a K type thermocouple. The thermocouple was bonded to the bottom of the sheet at a distance of 20 mm in the y direction from the start position of FSIF process by cyanoacrylate adhesive. The measurement results of the temperature of the sheet during FSIF process are shown in Fig. 15. The temperature of the sheet increased as the rod-shaped tool approaches to 5 mm in the y (horizontal) direction from the measurement point. The maximum temperature of the sheet reached approximately 433 K in FSIF process with ω = 6000 rpm. The temperature of the sheet increased higher than the glass transition temperature of PMMA (373 K) for longer than 10 s in FSIF process with ω = 6000 rpm. On the other hand, the maximum temperature of the sheet reached approximately 353 K, which did not reach the glass transition temperature of PMMA in FSIF process with ω = 1000 rpm.

The PMMA sheet was locally heated up to higher than the glass transition temperature of PMMA by the friction between the rod-shaped tool with a high rotation rate and the sheet. The strength of PMMA at the glass transition temperature was approximately 1/5 times of that at room temperature, and the viscosity significantly decreased at approximately 400 K (Bernhardt, 1959). The PMMA softened at higher than the glass transition temperature was vertically pushed and plastically flowed into the porous structure of the nickel foam by the rod-shaped tool, so that the foam was mechanically interlocked (anchored) with the sheet. This is the similar phenomenon with plastic flow of

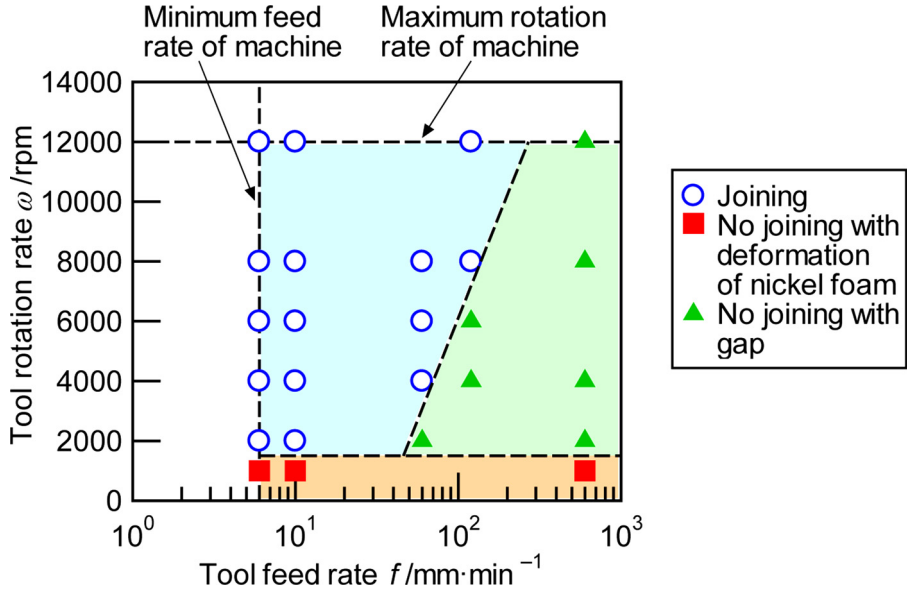

Fig. 7. Relationship between FSIF conditions and joining state of nickel foam–PMMA sheet after FSIF process.

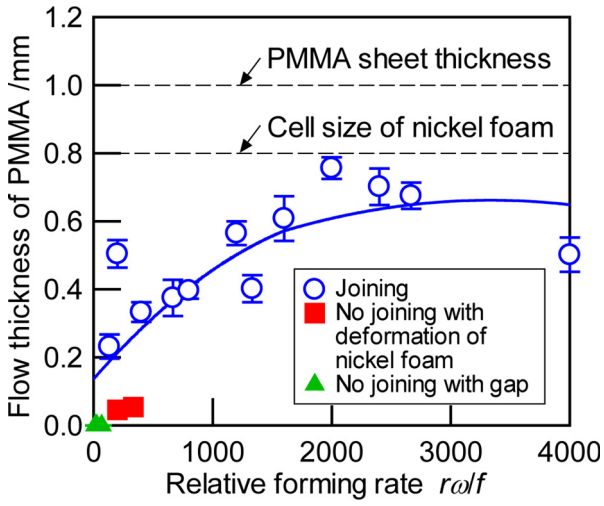

Fig. 8. Measurement results of flow thickness of PMMA sheet into porous structure of nickel foam plotted against relative forming rate of FSIF process.

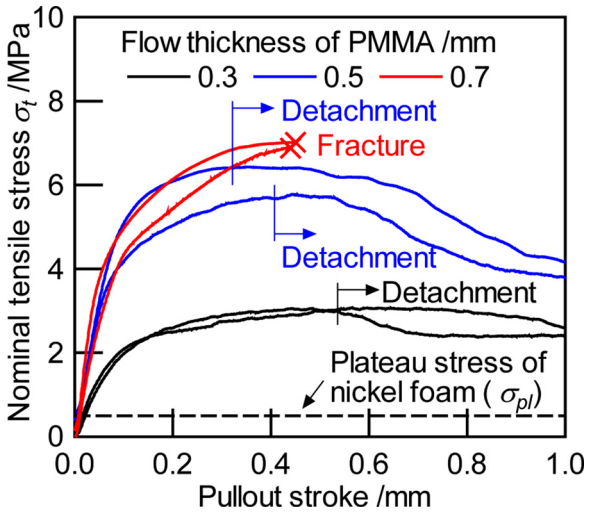

Fig. 10. Nominal tensile stress–pullout stroke curves of nickel foam joined with PMMA sheet in tensile test.

aluminum plate in friction-stir forming for fabrication of low-height and ultra-thin fin (Ohashi et al., 2017).

5.2. Shape of surface groove in plate

The plastic flow of the PMMA sheet and the mechanical interlock (anchor) of the PMMA and the porous structure of the foam were demonstrated by FSIF process of an aluminum plate with a groove and the PMMA sheet. The aluminum plate was commercially pure aluminum (JIS: A1100). The width and surface angle of the groove (see Fig. 16(b)) of the aluminum plate were 1.0 mm and $\alpha = 45^\circ$, 90° and 135°, respectively. FSIF conditions were $\omega = 6000$ rpm and $f = 10$ mm/min.

The photographs of the x–z cross-section of the interface between the groove in the aluminum plate and the PMMA sheet after FSIF process are shown in Fig. 16. The PMMA sheet plastically flowed into the groove and filled in the entire width direction of the groove, however the PMMA sheet was not joined with the aluminum plate with groove of $\alpha = 45^\circ$ and 90°. In the groove with $\alpha = 135^\circ$, PMMA flowed into the backside of the surface of the groove. Thus it is concluded that PMMA sheet was mechanically interlocked to the surface groove.

5.3. EDX analysis of joined interface

Fig. 17 shows the element map of the x–z cross-section of the interface of the nickel foam–PMMA sheet joined by FSIF process. The element map was obtained by energy dispersive x-ray spectrometry (EDX) analysis. The distributions of nickel and PMMA (carbon) were clearly detected in Fig. 17. The compound of nickel and PMMA was not detected at the interface between the foam and the sheet. In laser joining process of resin and aluminum substrate, Lamberti et al. (2014) and Okada et al. (2014) mentioned that the bonding was mainly due to mechanical interlock by the micro surface topology of the substrate or the resin. In FSIF joining of the nickel foam and the PMMA sheet, it is concluded that the chemical reaction contributed to the joining strength between nickel and PMMA was not caused at the interface.

6. Conclusions

Friction stir incremental forming (FSIF) process was applied to join a commercial open-cell type nickel foam with a polymethyl methacrylate (PMMA) sheet for fabrication of porous metal–nonporous resin composite. The relationship between the FSIF conditions and the joining strength was investigated. The joining mechanism of the foam and the sheet was discussed. The following remarks were obtained.

(1) The sheet was joined with the foam under FSIF conditions with rotation rate of the tool faster than 2000 rpm and feed rate of the tool slower than 60 mm/min.
(2) The joining strength between the foam and the sheet was over the fracture strength of the foam.
(3) The sheet was locally heated up to higher than glass transition temperature of PMMA by the friction between the rod-shaped tool with a high rotation rate and the PMMA sheet. The PMMA softened

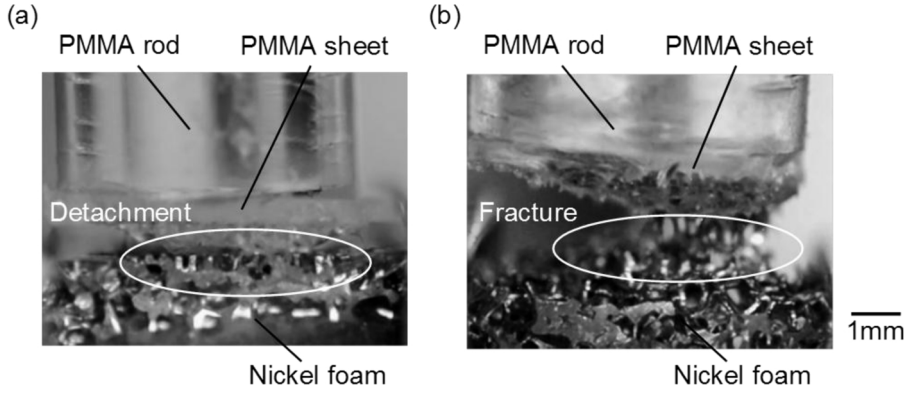

Fig. 9. Photographs of interface of nickel foam and PMMA sheet during tensile test: (a) detachment of PMMA sheet from nickel foam (flow thickness of PMMA: 0.5 mm), (b) fracture of nickel foam (flow thickness of PMMA: 0.7 mm).

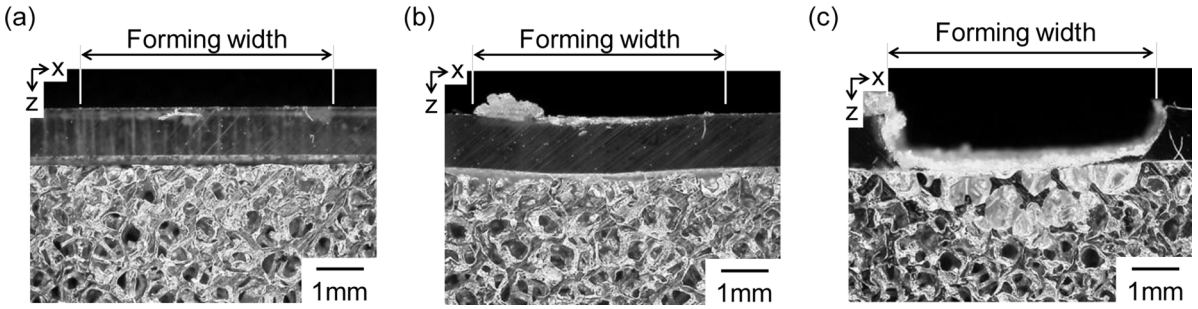

Fig. 11. Photographs of x–z cross-section of interface of nickel foam–PMMA sheet after FSIF process of a sheet thickness of 1.0 mm with ω = 6000 rpm and f = 10 mm/min: (a) p_z = 0.1 mm (no joining), (b) p_z = 0.3 mm (no joining), (c) p_z = 0.7 mm (joining).

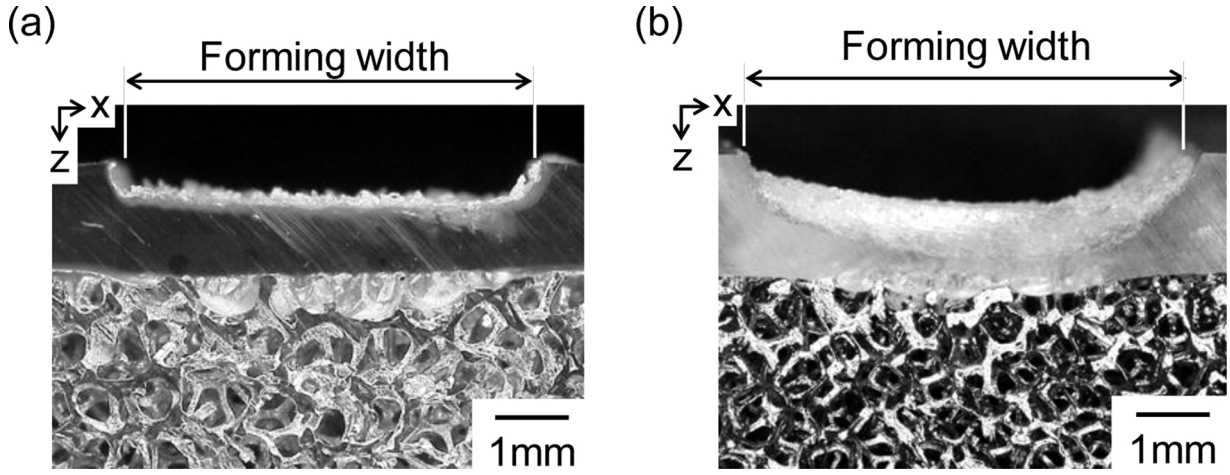

Fig. 12. Photographs of x–z cross-section of interface of nickel foam–PMMA sheet after FSIF process under ω = 6000 rpm, f = 10 mm/min and p_z = 0.5 mm: (a) sheet thickness: 1.5 mm (joining), (b) 2.0 mm (no joining).

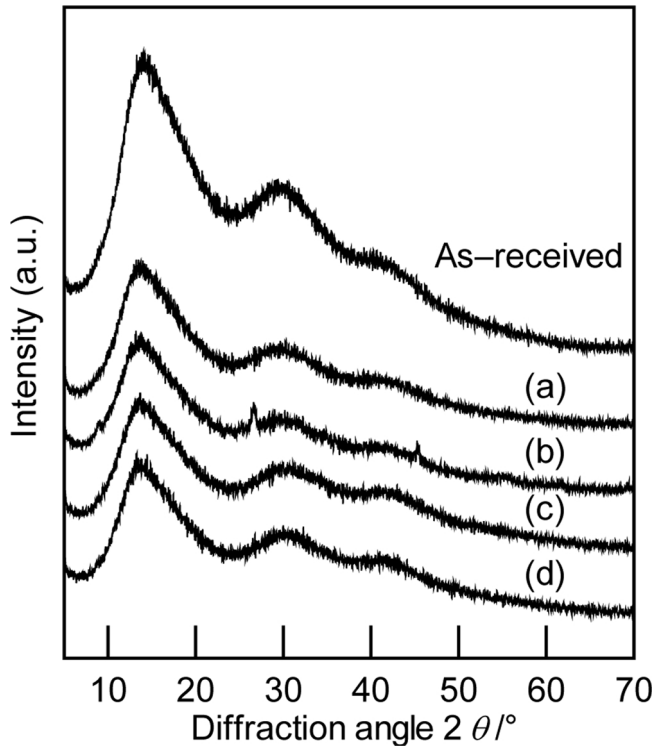

Fig. 13. X-ray diffraction pattern from x–y surface of PMMA sheet after FSIF process: (a) ω = 6000 rpm, f = 10 mm/min (joining), (b) ω = 6000 rpm, f = 120 mm/min (no joining), (c) ω = 1000 rpm, f = 10 mm/min (no joining), (d) ω = 1000 rpm, f = 120 mm/min (no joining).

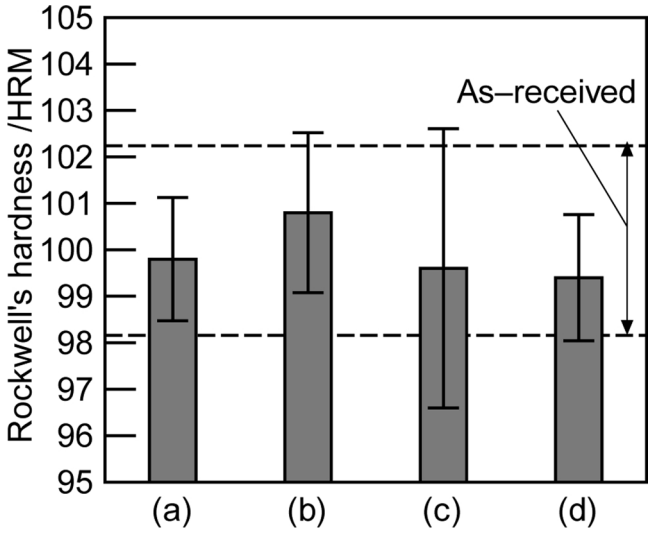

Fig. 14. Rockwell's hardness of x–y surface of PMMA sheet after FSIF process: (a) ω = 6000 rpm, f = 10 mm/min (joining), (b) ω = 6000 rpm, f = 120 mm/min (no joining), (c) ω = 1000 rpm, f = 10 mm/min (no joining), (d) ω = 1000 rpm, f = 120 mm/min (no joining).

at higher than the glass transition temperature was vertically pushed by the tool and plastically flowed into the porous structure of the nickel foam, so that the sheet was mechanically interlocked with the foam.

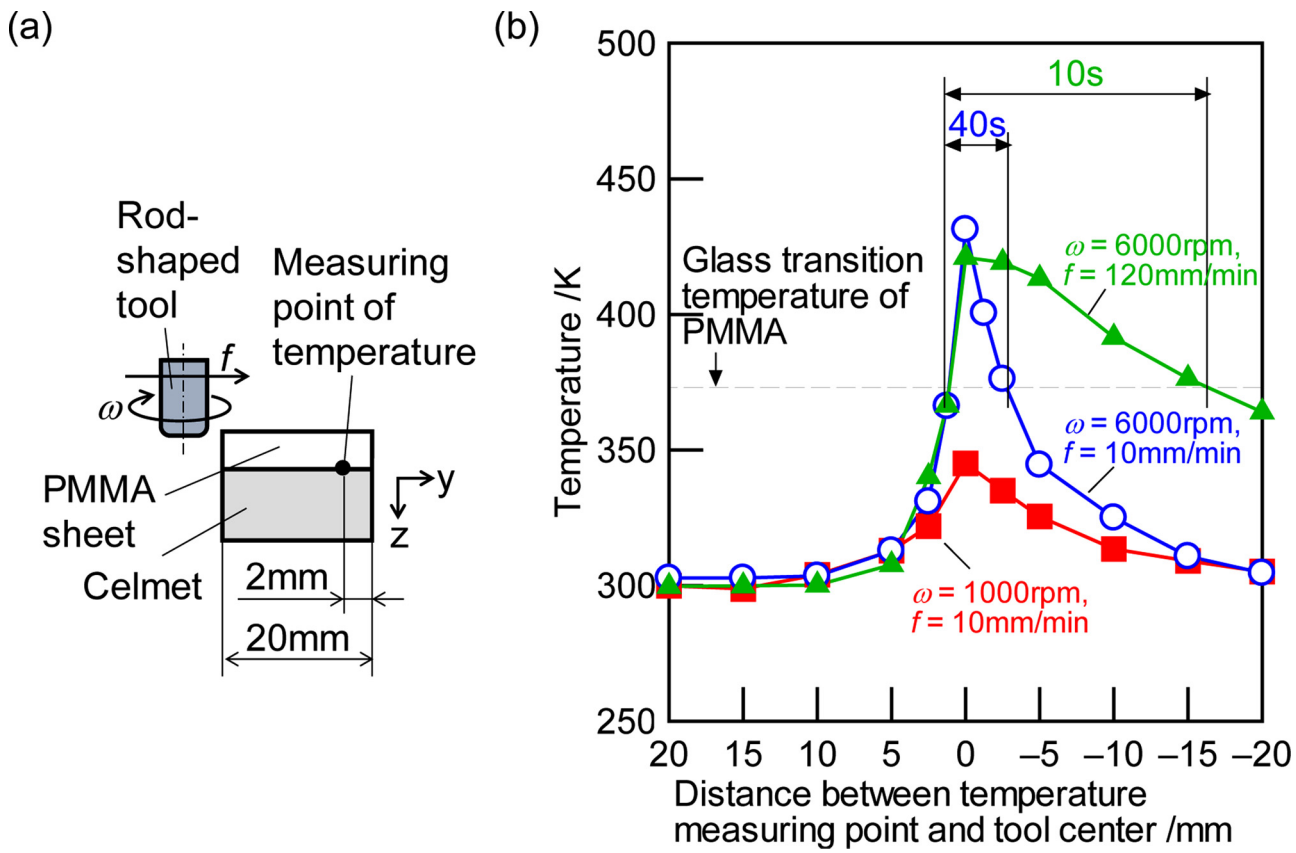

Fig. 15. Measurement results of temperature of PMMA sheet during FSIF process: (a) measurement point, (b) measurement results.

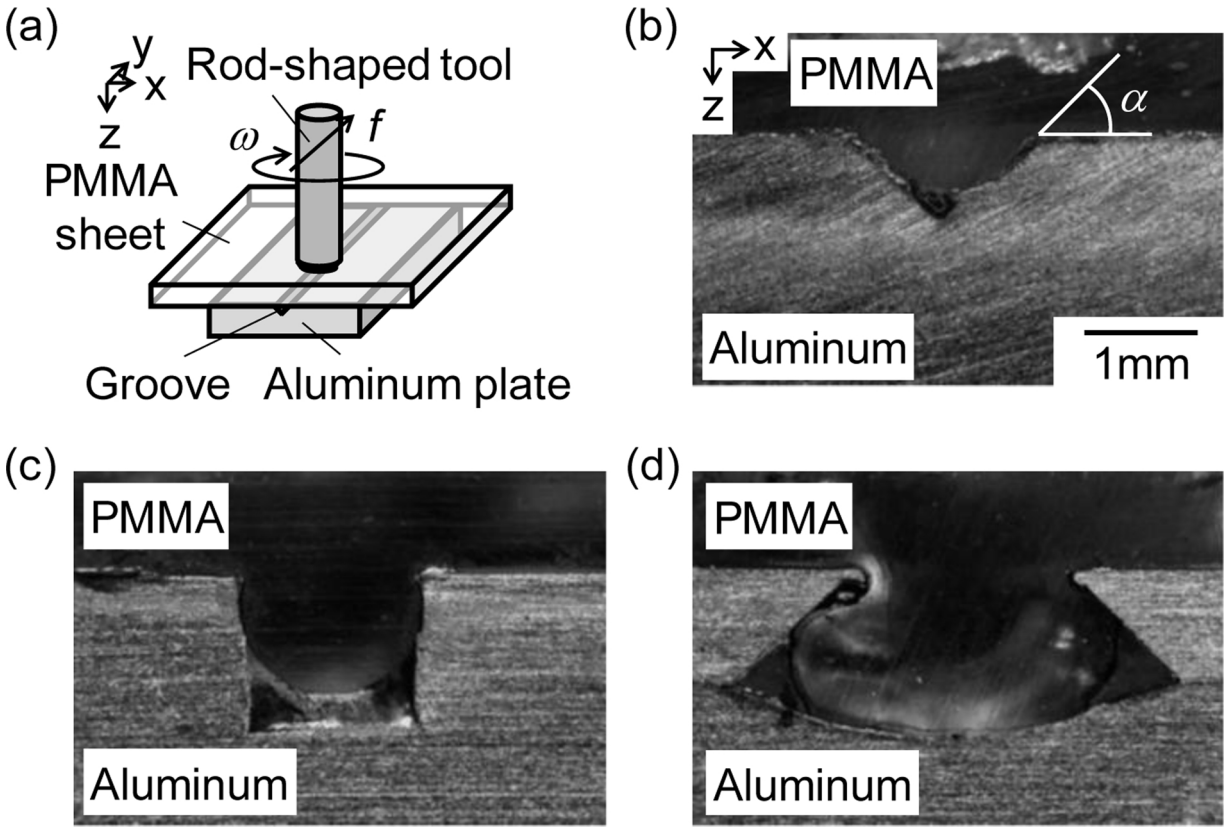

Fig. 16. Photographs of x–z cross-section of interface between groove in aluminum plate and PMMA sheet after FSIF process with ω = 6000 rpm and f = 10 mm/min: (a) schematic illustration of arrangement of tool, sheet and plate, (b) surface angle of groove: α = 45° (no joining), (c) α = 90° (no joining), (d) α = 135° (joining).

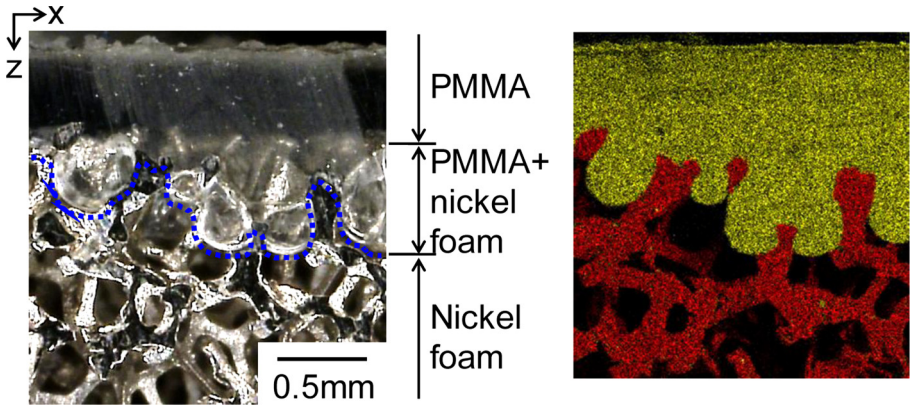

Fig. 17. Photograph and element map of x–z cross-section of interface of nickel foam–PMMA sheet joined by FSIF process with ω = 6000 rpm and f = 10 mm/min (green area: carbon, red area: nickel) (For interpretation of the references to colour in this figure legend, the reader is referred to the web version of this article.).

CRediT authorship contribution statement

Ryo Matsumoto: Conceptualization, Methodology, Formal analysis, Investigation, Data curation, Writing - original draft, Supervision. **Harutaka Sakaguchi:** Investigation, Data curation, Visualization. **Masaaki Otsu:** Validation, Writing - review & editing. **Hiroshi Utsunomiya:** Validation, Writing - review & editing.

Declaration of Competing Interest

The authors declare that they have no known competing financial interests or personal relationships that could have appeared to influence the work reported in this paper.

Acknowledgement

This study was financially supported in part by the Light Metal Educational Foundation, Inc. The author (R. Matsumoto) would like to thank Mr. S. Lee, graduate student of Osaka University for his help in use of x-ray diffractometer.

References

Ashby, M.F., Evans, A., Fleck, N.A., Gibson, L.J., Hutchinson, J.W., Wadley, H.N.G., 2000. Metal Foams: A Design Guide. Butterworth-Heinemann.
Banhart, J., 2001. Manufacture, characterization and application of cellular metals and metal foams. Prog. Mater. Sci. 46 (6), 559–632.
Bernhardt, E.C., 1959. Processing of Thermoplastic Materials. Reinhold Publishing Corporation.
Inazawa, S., Hosoe, A., Majima, M., Nitta, K., 2010. Novel plating technology for metallic foam. Sumitomo Electric Ind. (SEI) Tech. Rev. 71, 23–30.
Kajihara, Y., Tamura, Y., Kimura, F., Suzuki, G., Nakura, N., Yamaguchi, E., 2018. Joining strength dependence on molding conditions and surface textures in blast-assisted metal-polymer direct joining. CIRP Ann. Manuf. Technol. 67 (1), 591–594.
Katayama, S., Kawahito, Y., 2008. Laser direct joining of metal and plastic. Scr. Mater. 59 (12), 1247–1250.
Kim, S.G., Suzuki, A., Takata, N., Kobashi, M., 2019. Joining of metals and polymers using powder metallurgy with laser irradiation. J. Mater. Process. Technol. 270, 1–7.
Kim, W.Y., Matsumoto, R., Utsunomiya, H., 2017. Deformation and density change of open-cell nickel foam in compression test. Mater. Trans. 58 (10), 1373–1378.
Kitazono, K., Suzuki, R., Inui, Y., 2009. Novel strengthening method of closed-cell aluminum foams through surface treatment by resin. J. Mater. Process. Technol. 209 (7), 3550–3554.
Koriyama, S., Paiboon, S.-T., Suzuki, S., Asakawa, M., Ide, T., Nakajima, 2012. Enhancement of the hardness of lotus-type porous copper by shot peening. Steel Res. Int. 1215–1218 Special Edition.
Lakshminarayanan, A.K., Balasubramanian, V., Elangovan, K., 2009. Effect of welding processes on tensile properties of AA6061 aluminium alloy joints. Int. J. Adv. Manuf. Technol. 40 (3-4), 286–296.
Lamberti, C., Solchenbach, T., Plapper, P., Possart, W., 2014. Laser assisted joining of hybrid polyamide-aluminum structures. Phys. Procedia 56, 845–853.
Liu, Y., He, X., Deng, C., 2017. Self-piercing riveting of metal foam sandwich structures. Mater. Trans. 58 (11), 1532–1537.
Lobos, J., Suzuki, S., Nakajima, H., Ji, Y.S., Fujii, H., Terada, D., Tsuji, N., 2009. Structural change and improvement of the mechanical properties of a lotus-type porous copper by wire-brushing. J. Phys. Conf. Ser. 165, 012070.
Matsumoto, R., Tsuruoka, H., Otsu, M., Utsunomiya, H., 2015. Fabrication of skin layer on aluminum foam surface by friction stir incremental forming and its mechanical properties. J. Mater. Process. Technol. 218, 23–31.
Matsumoto, R., Kanatani, S., Utsunomiya, H., 2016. Filling of surface pores of aluminum foam with polyamide by selective laser melting for improvement in mechanical properties. J. Mater. Process. Technol. 237, 402–408.
Matsumoto, R., Mori, S., Otsu, M., Utsunomiya, H., 2018. Formation of skin surface layer on aluminum foam by friction stir powder incremental forming. Int. J. Adv. Manuf. Technol. 99 (5–8), 1853–1861.
Ohashi, T., Tabatabei, H.M., Nishihara, T., 2017. Low height ultra-thin fin on A5083 aluminum plate fabricated by friction-stir forming. Procedia Eng. 174, 74–81.
Okada, T., Uchida, S., Nakata, K., 2014. Direct joining of aluminum alloy and plastic sheets by friction lap processing. Mater. Sci. Forum 794-796, 395–400.
Otsu, M., Matsuo, H., Matsuda, M., Takashima, K., 2010. Friction stir incremental forming of aluminum alloy sheets. Steel Res. Int. 81 (9), 942–945.
Peng, P., Wang, K., Wang, W., Huang, L., Qiao, K., Che, Q., Xi, X., Zhang, B., Cai, J., 2019. High-performance aluminium foam sandwich prepared through friction stir welding. Mater. Lett. 236, 295–298.
Shiomi, M., Imagama, S., Osakada, K., Matsumoto, R., 2010. Fabrication of aluminium foams from powder by hot extrusion and foaming. J. Mater. Process. Technol. 210 (9), 1203–1208.
Suzuki, A., Arai, Y., Takata, N., Kobashi, M., 2018. Effect of layer thickness on bonding strength of Al/epoxy resin joints via interpenetrating phase layer. J. Mater. Process. Technol. 254, 338–345.
Wang, H., Yang, D., He, S., He, D., 2010. Fabrication of open-cell Al foam core sandwich by vibration aided liquid phase bonding method and its mechanical properties. J. Mater. Sci. Technol. 26 (5), 423–428.
Yuan, J., Chen, X., Zhou, W., Li, Y., 2015. Study on quasi-static compressive properties of aluminum foam-epoxy resin composite structures. Compos. Part B Eng. 79, 301–310.